

Design of Vortex Generator Flow Control in Inlets

Adam Jirásek*

Swedish Defence Research Agency FOI, 164 90 Stockholm, Sweden

DOI: 10.2514/1.21364

This article summarizes the results of an optimization study of a microvortex generator flow control in an inlet. Five parameters optimization was carried out using the classical design of experiment method. Two main objectives were in focus: first, to develop the methodology and skills necessary to conduct a design of experiment optimization study in area of the flow control; and second, to develop the procedures which would be used during design of vortex generator flow control in inlets. New information about the dependency of the vortex generator flow control in inlet on its geometrical parameters were obtained. Several interesting configurations were located. The parameters of optimal settings were then used to set up the vortex generator installation in a generic inlet.

Nomenclature

DC_{60}	= pressure distortion
h	= vortex generator height
l	= vortex generator length
M	= Mach number
p_r	= pressure recovery
R	= throat radius
s	= vortex generator spacing
x_s	= location of the flow separation
α_c	= circumferential angle of VG row
α_p	= inclination angle of a VG row plane
α_{VG}	= angle of incidence of vanes
Δx	= distance of the VG row from separation
δx	= boundary layer thickness

Subscript

c	= coded values
-----	----------------

I. Introduction

THE S-duct diffusers become an integral part of the design of a new aircraft. Their potential benefit includes shorter and lighter construction of inlet, reduction of the pressure losses or buried engine concept [1–3]. Interesting is also a combination of a short S-duct with boundary layer ingestion which can bring a reduced fuel consumption [4,5]. Especially for military applications, S-ducts reduce radar cross-sectional visibility by covering the engine face [1,3]. The major problem of these inlets is the flow separation. This separation, which is a consequence of a high curvature of the inlet walls, gives rise to losses and contributes to the flow distortion. The consequence is a severe problem caused to the engine functionality such as reduction of surge margin, exceeded turbine nozzle and blade temperature limits, promoted forced compressor rotor vibration and coupled blade-disk-mode excitation, increased stator stress loads, and affected compressor flutter onset limits [6]. To reduce the flow separation in S-ducts, Kaldschmidt et al. [7] proposed using a set of vortex generators (VGs) located in the inlet which restructure the flowfield in inlet. The idea has then been further studied by others [2,8–14]. These studies indicated very strong dependence of the

functionality of the VG flow control on the setting of its geometrical parameters. Some VG installations have been certainly found using a pick-up winner design or by a one-factor-at-a-time design. Although simple, these designs lack or have rather limited amount of information about the system response on the changes of design variables. More advanced designs such as the design of experiment (DOE) [15,16] or designs constructed for computer simulations denoted as modern DOE or design and analysis of computer experiment (DACE) [17] can give more complex answer. To the author's knowledge, previous DOE studies with the VG flow control in S-duct without and with boundary layer ingestion have been carried only in the United States: see [2,11–13,18–22]. Some of these studies are interesting in including both geometrical and flow parameters such as Reynolds number and angle of inlet incidence [18,19,22]; some of them included boundary layer ingestion [11–13]. Most of these studies included up to four geometrical parameters and almost all indicate very strong dependence on the vortex generator height.

This paper summarizes the results of flow control optimization study in the RAE M2129 S-duct using CFD simulations and DOE. It extends the number of design parameters to five. Two main goals were in focus. First, to make preliminary study on VG flow control taking to account several design parameters, determine their possible limits, carry out the screening experiment and construct the response surface (RS). This should extend the understanding of system behavior and can increase knowledge on VG flow control. Second, to develop a methodology and skills which can be used for future studies of real geometries using classical DOE methods. Only geometrical parameters were chosen. The difficulties with mesh generation of inlets with a large number of VG configuration were avoided by employing a vortex generator model [23]. It models the effect of VGs rather than embeds the shape into the computational mesh. It enabled to large extent the study presented in this paper. The findings from analysis of RS were then used to design vortex generator flow control in an unmanned aerial vehicle (UAV).

II. Design of Experiment Methodology

"Statistical design of experiment refers to the process of planning the experiment so that appropriate data that can be analyzed by statistical methods will be collected, resulting in valid and objective conclusion" [24].

Classical DOE methods have been used successfully for several decades. The DOE term covers the system of methods that are used to build a relation between several input design parameters and one or several responses. The DOE is most commonly used to analyze the data obtained through experiments which enables independent error estimate by randomly repeating one or several runs. This design is called replicated design. Some types of experiments do not enable repeatability, for example, too costly experiments or deterministic computer simulations. The design is then called unreplicated design.

Presented as Paper 1050 at the 44th AIAA Aerospace Sciences Meeting and Exhibit, Reno, NV, 9–12 January 2006; received 24 November 2005; revision received 30 August 2006; accepted for publication 5 September 2006. Copyright © 2006 by FOI. Published by the American Institute of Aeronautics and Astronautics, Inc., with permission. Copies of this paper may be made for personal or internal use, on condition that the copier pay the \$10.00 per-copy fee to the Copyright Clearance Center, Inc., 222 Rosewood Drive, Danvers, MA 01923; include the code \$10.00 in correspondence with the CCC.

*Research Engineer; Division of Systems Technology; Adam.Jirasek@foi.se. Member AIAA.

In the literature, the use of unreplicated design is not generally recommended and if used it is usually considered as a part of the screening process. However, the unreplicated design with computer simulations becomes an important option in the optimization process. The analyst who decides to use DOE together with computer simulations for conducting the design must therefore be aware of the limitation of unreplicated design and carefully use many different diagnostics techniques together with a number of verification runs to check the RS model adequacy. Another option may be to use a family of designs developed for analysis of computer simulations called DACE modeling [17,25,26].

For the modeling part of the DOE a large number of fractional factorial designs have been developed, such as Latin square design, Box–Behnken, Box–Wilson or central composite design (CCD), D-optimal design, etc. One of the most popular design is the CCD design. It is a design that evolves in sequential experimentation. The design accommodates a spherical region with five levels of each factor. It uses the two-level fractional or fraction factorial design combined with the axial and central points. Its specific form is a design with three levels for each factor, called face center cube of central composite face design (CCF). A different type of design is a Taguchi design, which splits factors to controllable factors and noise. It is so called robust design, which determines factor settings to optimize the response and minimizes variability. It uses crossed arrays, inner array for controllable factors and outer array for noise factors. In the CFD, this design can be used for a combination of geometrical and flow parameters. The disadvantage of the Taguchi design is that it requires a large number of runs due to cross-arrays which can be reduced by using so-called combined arrays. For more details see literature [15,16,24].

III. Flow Solver

The CFD flow solver used for this study is Edge [27], a finite volume Navier–Stokes solver for unstructured meshes. It employs local time-stepping, local low-speed preconditioning, multigrid and dual-time-stepping for steady-state and time-dependent problems. The data structure of the code is edge-based so that the code is constructed as cell-vertex. It can be run in parallel on a number of processors to efficiently solve large flow cases. It is equipped with a number of turbulence models based both on the eddy-viscosity and an explicit algebraic Reynolds stress model (EARSM) assumption. The model that was used during this study was the two-equation $k-\omega$ model combined with EARSM model [28] with compressible corrections. Vortex generators were modeled using a vortex generator model [23]. The code has a number of boundary conditions for inlet and outlet boundaries. The one used for an inlet boundary was total states inlet or mass flow inflow boundary condition. For an outlet, the static pressure or outflow mass flow boundary conditions were used [29].

The CFD calculations were stopped after the changes of residuals, pressure recovery, and pressure distortion were negligible. Particularly the pressure distortion seems to be a very sensitive indicator of convergence.

IV. Optimization Study of the RAE M2129 Channel

A. Definition of Experiment

The test case in which the DOE design of flow control is used is the RAE M2129 channel [30]. The two values in the aerodynamic interface plane (AIP) were recorded: pressure recovery p_r and circumferential pressure distortion index DC_{60} [31]. The flow was calculated for a throat Mach number of $M = 0.66$ and a mass flow through channel $\dot{m} = 22.615 \text{ kg/s}$ and at total temperature $T_0 = 300 \text{ K}$ at inflow boundary. The final value of pressure distortion is $DC_{60} = 56.90\%$ and pressure recovery $p_r = 96.457\%$. Figure 1a shows the streamlines at the surface and pressure recovery in the AIP for the channel without flow control. A large area of pressure loss at the lower part of the channel gives rise to high circumferential pressure distortion and to high pressure losses. Figure 1b shows fully attached flow through channel with VG flow control.

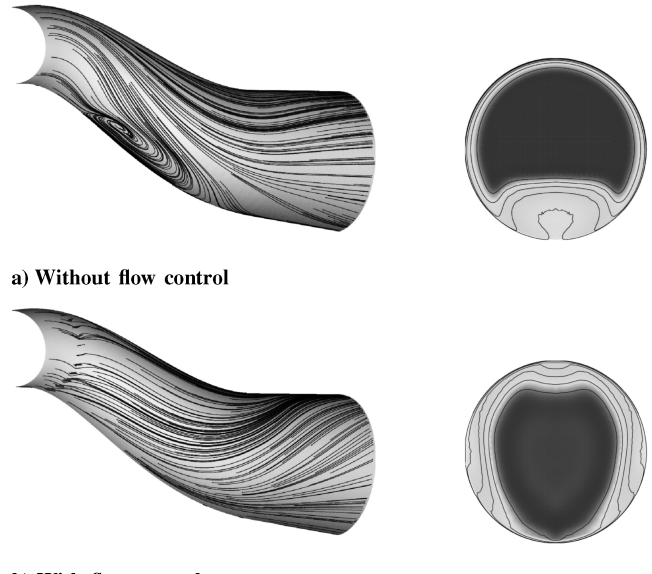


Fig. 1 Surface streamlines and pressure recovery in the RAE M2129 S-duct.

The optimization study on VG flow control was carried out with geometrical parameters schematically shown in Fig. 2. No flow parameters such as Mach or Reynolds number were included. The reason is to avoid having the boundary layer thickness in the response surface as an unknown function of the flow parameters. Rather, the boundary layer thickness effect is included via a parameter h/δ .

Two sets of design parameters were used. In previous works mentioned in the Introduction, some authors used pure geometrical parameters; others tied the geometrical parameters to the boundary layer height. The motivation of using two sets in this study is to determine which one gives a better result. The first set includes the vortex generator height h , the vortex generator relative length l/h , the vortex generator relative spacing s/h , the relative distance of VG row from separation $\Delta x/h$, and the inclination angle of VG row α_p . Because the l , s , and Δx parameters are normalized by vortex generator height h , this set is called the set of nondimensional parameters. The second set consists of the vortex generator height h , vortex generator length l , vortex generator spacing s , distance of the VG row from separation Δx , and the inclination angle of VG row α_p . This set is called the set of dimensional parameters. All vortex generators have a rectangular shape. Two direct consequences of the different choice of design parameters can be seen. First, the set of nondimensional parameters ties all longitudinal parameters to the boundary layer height. Second, because classical DOE distribute most points on the perimeter of the design space, the choice of a definition of the design parameters affects the distribution of the vortex generators in the channel. Figure 3 shows the distribution of planes with vortex generators in the channel for all tested configurations. The apparently better space filling property of the nondimensional set can be seen in Fig. 3a. A consequence of using the nondimensional set of parameters is the reduced distance of the VG row from the flow separation, $\Delta x/h$, for lower vortex generators. Fortunately, as shown later, the interesting configurations are those

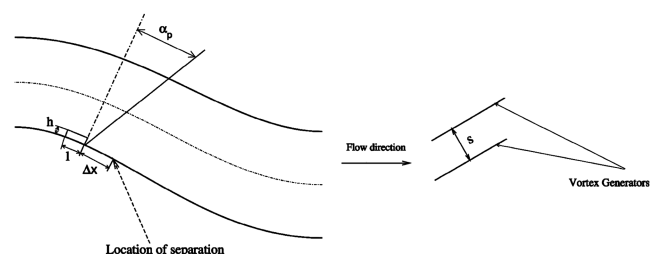
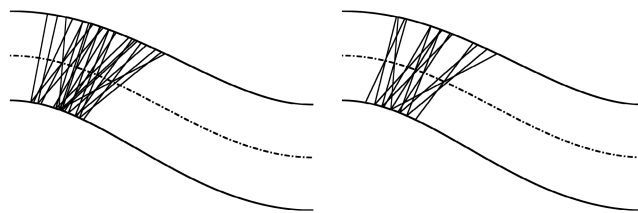


Fig. 2 Geometrical parameters in the RAE M2129 S-duct.



a) Nondimensional set of parameters

b) Dimensional set of parameter

Fig. 3 Position of VG rows in the RAE M2129 S-duct for all configurations.

located close to flow separation. For both sets the vortex generator angle of incidence was kept constant at $\alpha_{VG} = 25$ deg. Tables 1 and 2 summarize design variables and their limits. The lower and upper limits of both sets were chosen so that the minimum and maximum value of h , l , s , Δx , and α_p , are identical for both design matrices.

B. CCD Design Matrix and RS Methodology

The design chosen for this study is central composite design. Its choice was determined by a larger number of design factors, by its ability to be run sequentially, and by rotatability feature. The chosen CCD design matrix for five design factors contains 27 runs where the first 16 runs belong to the factorial part of the design, one run is the central point, and 10 runs are on the axial part of the design. The factorial part of the design matrix is a fractional factorial, resolution R_V design with definition equation $I = ABCDE$. It may complicate analysis but it is believed that the four order interactions are very possibly unimportant. The central and axial runs also contribute to dealiasing of this interactions from the primary factors. If it is necessary it is possible to add sequentially the remaining eight runs to the fractional part of the design.

The values of pressure distortion and pressure recovery were used to build a RS using least square method. The procedure is described in [15]. It contains linear and quadratic terms of the factors and their interactions. The data of DC_{60} were, due to high scatter, transformed by logarithmic transformation. The diagnostics include the test for significance of regression, R^2 and R^2_{adj} and the t-test of individual regression coefficients. The model adequacy checking includes residual analysis of the values of residuals, studentized residuals and PRESS residuals, Hat matrix coefficient, and Cook's distance [15]. Furthermore, the plot of residuals vs predicted value, the normal probability plot of residuals, and the normal probability plot of studentized residuals were used also [32,33].

C. Analysis of CCD Matrix Data Results

1. Set of Nondimensional Variables

Figure 4 shows the distribution of pressure recovery in the AIP for all cases defined by the set of nondimensional variables. Focusing on

Table 1 Nondimensional parameters limits

Factor	Lower limit	Upper limit
Height h/δ , %	20	50
Relative length l/h	6	12
Relative spacing s/h	2	5
Relative distance $\Delta x/h$	0	27
Inclination angle α_p , deg	-10	50

Table 2 Dimensional parameters limits

Factor	Lower limit	Upper limit
Height h/R^a , %	20	50
Length l/R^a	0.252	0.630
Spacing s/R^a	0.098	0.252
Distance $\Delta x/R^a$	0	1.323
Inclination angle α_p , deg	-10	50

^aLongitudinal parameters are nondimensional with inlet radius R as a reference length.

the factorial part of the design (runs 1–16) in Fig. 4, one can see that runs 9–16, which correspond to lower vortex generators, give more favorable distribution of pressure losses along the wall. It may be therefore expected that lower vortex generators have better performance. The axial part of the design shows the apparent effect of vortex generator height h (runs 18, 17, 19) and of the distance of the vortex generator row from the separation Δx (runs 24, 17, 25). The effect of other parameters on the distribution of pressure recovery is rather difficult to see.

The values of residuals, studentized residuals, Hat matrix coefficient, and Cook's distance do not indicate any potential problem with the RS. The same conclusion can be made from the plot of residuals vs predicted value: Fig. 5a. Normal probability plots of residuals in Fig. 5b and normal probability plots of studentized residuals in Fig. 5c give a mild indication that the errors come from a distribution with heavier tails than the normal. Because there is no strong indication of model inadequacy, the conclusion is that the model is satisfactory [34]. The same conclusion can be made for the RS made of pressure recovery values.

The analysis of the RS for pressure distortion DC_{60} is shown in Table 3, which shows the t-values for the six most significant terms. Apparently the most important parameters are the vortex generator height h and the distance of the vortex generator row from the separation $\Delta x/h$ and their interactions. Vortex generator length l/h and vortex generator spacing s/h seem to have a mild effect on distortion, especially for lower vortex generators. A surprising finding is that the inclination angle of the VG row plane, α_p , is an unimportant factor. Figure 6 shows graphically the examples of the dependence of pressure distortion on the three design factors l/h , s/h , and $\Delta x/h$ for different vortex generator heights h . It seems that from the pressure distortion point of view, generally the low vortex generators located close to the separation are preferable.

The values of the pressure recovery p_r do not differ very much. The largest benefit in the pressure recovery was obtained by reducing the flow separation in the channel. Once the flow separation is reduced, the major source of pressure losses is the VG flow control system itself due to friction losses on the vortex generators and blockage effect. At this stage, the changes of the VG setup between

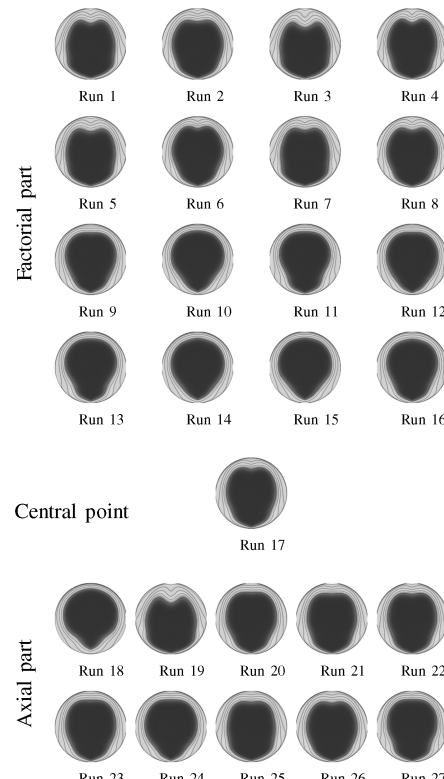


Fig. 4 Pressure recovery in the RAE M2129 S-duct for 27 configurations.

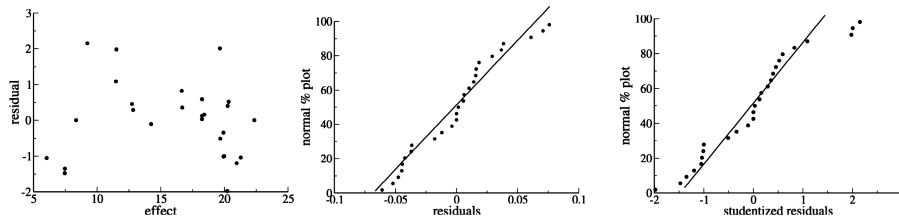


Fig. 5 Diagnostic plots for DC_{60} response surface.

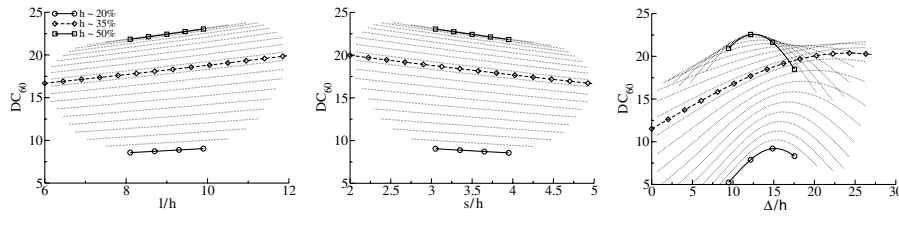


Fig. 6 DC_{60} in the AIP in the RAE M2129 S-duct.

different configurations do not have a large effect. The analysis of the pressure recovery RS shows that the two most important terms are h^2 and angle of inclination plane α_p and their interactions. Table 4 shows the t-values for the six most significant terms in the RS of the pressure recovery. Analogical set of graphs as for the pressure distortion showing p_r as function of design parameters were made and are shown in Fig. 7.

2. Set of Dimensional Variables

During the attempts to build the RS for set of the dimensional parameters, the normal probability plot indicated serious problems of the RS for pressure distortion. Furthermore the RS failed predicting one verification run, which all together indicates that the RS model is inadequate. A possible reason might be a strong dependence of the pressure distortion on the term l/h . Another reason can be the space filling property of the design. The set of dimensional parameters was therefore excluded from further study.

D. Results of Optimization Study

Both the pressure distortion and pressure recovery RS for nondimensional set of parameters were used to locate the optimal point. This point is characterized as the one with high pressure recovery and $DC_{60} < 10\%$. The parameters of this configuration are $h = 27.5\%\delta$, $l/h = 8.25$, $s/l = 3.5$, $\Delta x/h = 6.75$, and $\alpha_p = 20$ deg. Its layout is shown in Fig. 8. Predicted values were $DC_{60} = 7.08 \pm 0.98\%$ and $p_r = 97.120 \pm 0.018\%$. The final values of the pressure recovery and pressure distortion, found by running the CFD calculations, were $p_r = 97.115\%$ and $DC_{60} = 6.50\%$, respectively. Both values are located inside the

interval of confidence. Compared to the results of the flow through the inlet without vortex generators, the DC_{60} was reduced from $DC_{60} \approx 56\%$ to about $DC_{60} \approx 7\%$ and the pressure recovery increased by $\approx 0.66\%$, from $p_r = 96.46\%$ to $p_r = 97.12\%$.

Another configuration represents an attempt to move the VGs deep into the channel. It is required that the VG configuration should have high pressure recovery and DC_{60} below 10%. The distance of this configuration Δx is fixed at the lowest limit of the design space, $\Delta x/h = 0$, and inclination angle at the highest limit, $\alpha_p = 50$ deg. The other three remaining parameters were found using tendencies shown by RS for pressure distortion and pressure recovery and their values are $h = 30\%\delta$, $l/h = 6$, and $s/h = 5$. Figure 9a shows the position of the VG row in the channel. It must be mentioned that this approach means an extrapolation outside the design region and is generally not recommended. The final values of pressure distortion and pressure recovery found from the CFD solution are $DC_{60} = 5.67\%$ and $p_r = 97.056\%$. Figure 9b shows the pressure recovery in the AIP of the channel for this configuration.

A note can be made here. The vortex generator flow control used in this article has four parameters which are strongly tied to the local flow properties: local boundary layer height δ and the location of flow separation in the channel x_s . Two of these parameters, h and Δx , are dominant whereas the other two parameters, l and s , have a mild effect. A fifth parameter, the inclination angle of the VG row plane, α_p , which is independent of any flow parameters, has no effect on distortion. It suggests that there may be a possibility to define active VG flow control with two input variables: δ and x_s . Their recording is relatively easy and they can be sampled using a high sampling rate. The main advantage is that because the VG flow control is located close to the location where δ and x_s are sampled the feedback of the control system can be relatively simple.

Table 3 Table of significance for RS for DC_{60} , $t^* = 2.160$

Term	t-value
DC_0	-84.3522
h	13.0506
$\Delta x/h$	12.9185
Δx	-9.6244
Δx^2	-6.9257
h^2	-6.7585
$\Delta x/h$	4.9012
s/h	4.1936

Table 4 Table of significance for RS for p_r , $t^* = 2.262$

Term	t-value
P_{r0}	>1000
α^2	-15.9301
α	-12.2232
Δx	6.6845
$\Delta x\alpha$	5.0319
l/h	4.4284
s/h	4.1599

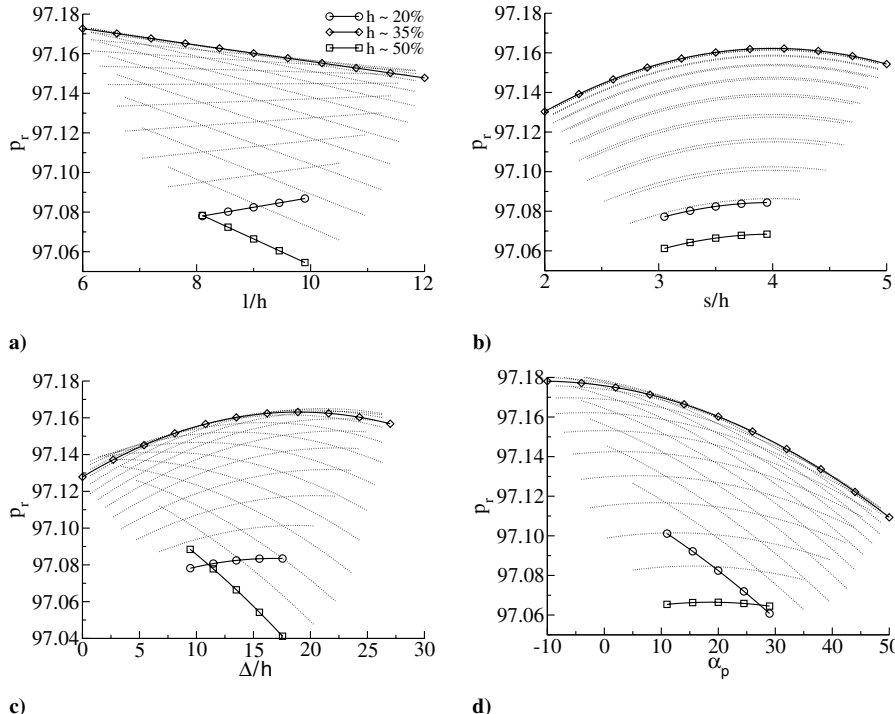
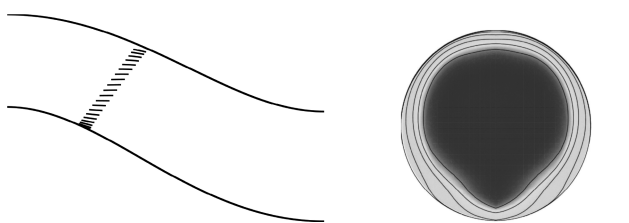


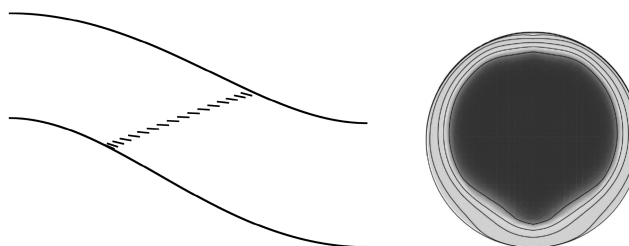
Fig. 7 Pressure recovery in the AIP in the RAE M2129 S-duct.



a) Position of a plane with vortex generators

b) Pressure recovery in the AIP plane

Fig. 8 Optimal VG configuration in the RAE M2129 S-duct.



a) Position of a plane with vortex generators

b) Pressure recovery in the AIP plane

Fig. 9 Most downstream VG configuration in the RAE M2129 S-duct.

V. Application Case

A. FOI-EIC-01 UAV inlet

The optimal settings of parameters defining the vortex generator setup derived in Sec. IV.C were used to design a vortex generator flow control in the FOI-EIC-01 UAV inlet. This work has been supported by the Swedish Defence Materiel Administration, FMV, and carried out within the common FOI, Volvo Aero Corporation and SAAB Aerospace project called Propulsion Integration project [35]. The shape of the channel is shown in Fig. 10.



a) Wind tunnel model of the inlet with b) FOI-EIC-01 inlet geometry forebody

Fig. 10 Inlet and UAV aircraft geometry.



Fig. 11 Two vortex generator installations in FOI-EIC-01 inlet.

Because at the time of this study the shape of forebody was not known, the mesh contains simple upstream extension to build an appropriate boundary layer. The boundary conditions for this case were mass flow boundary condition at the inlet and Mach number boundary condition at the outlet [29]. The vortex generators were modeled using the VG model. The results shown here were calculated at mass flow $\dot{m} = 60 \text{ kg/s}$ and average Mach number in the AIP $M = 0.5$.

The channel without flow control exhibits intense flow separation behind the second bend: Fig. 11, which is the main source of the flow distortion. The location of the flow separation on the upper side of the channel is rather stable due to high curvature of the surface. An area of lower total pressure recovery is present on the lower side of the channel shortly after the first bend; however, the flow there is not separated. There is a vortical structure visible along the channel wall which gives rise to a small disturbance of total pressure in the lower part of the AIP. It is a result of high curvature at the beginning of the channel.

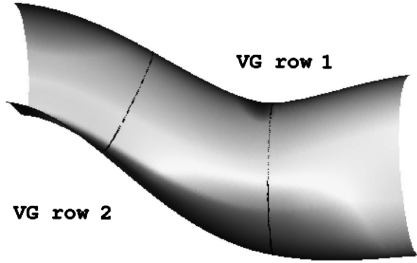
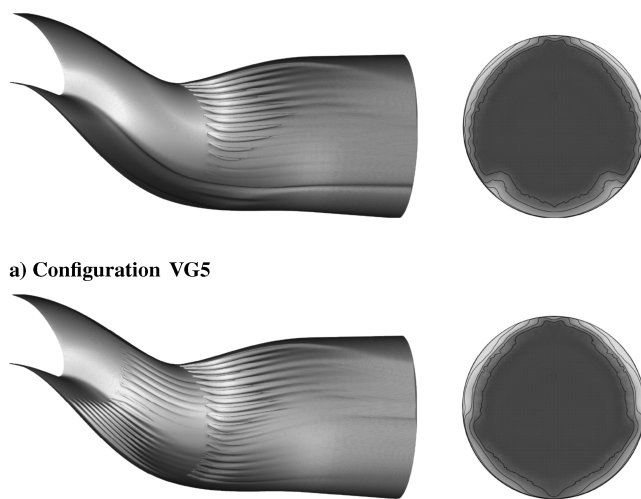


Fig. 12 Position of vortex generator rows in the channel.



a) Configuration VG5
b) Configuration VG9
Fig. 13 Isosurface of total pressure and pressure recovery in the AIP, FOI-EIC-01 inlet.

Two vortex generator setups with rectangular vortex generators were designed: Fig. 12. The first setup, denoted as VG5, has one row of vortex generators, denoted VG row 1 located in upstream of the flow separation. The second setup, denoted as VG9, has two rows of vortex generators. It keeps VG row 1 from the VG5 setup and adds the second VG row 2 upstream of the first bend. The reason for designing VG9 configuration was to reduce possible separation of the flow caused by ingested boundary layer from the forebody of the plane. Both configurations have vortex generator height $h = 30\% \delta$ of the boundary layer height, length $l/h = 7.5$, and spacing $s/h = 6.1$. The angle of the vanes in the VG row 2 was set to $\alpha_{VG} = 20$ deg and of the VG row 1 to $\alpha_{VG} = 10$ deg. The choice of

Table 5 Pressure distortion, total pressure recovery, VG9 configuration

Configuration	DC_{60} , %	p_r , %
Baseline	57.13	96.45
VG5	2.97	98.42
VG9	5.96	98.30

Table 6 Total pressure recovery and DC_{60} , wind tunnel test

Re	No VGs		With VGs	
	p_r	DC_{60}	p_r	DC_{60}
2.9×10^6	94.7	56.2	94.6	24.3
5.9×10^6	95.1	53.5	95.4	11.5
7.0×10^6	95.1	52.5	95.3	21.6

the lower angle of vane incidence in the VG row 2 was motivated by avoiding generating too strong secondary motion from the lower to the upper side of the inlet. Too strong redistribution of the flow generated by VG row 2 can worsen the flow upstream of the VG row 1. The value of relative spacing s/h is larger than the value defined for optimal configuration in the RAE M2129 channel. A mild dependence of the pressure distortion on the spacing justifies a larger value of spacing.

Both vortex generator installations successfully eliminated the flow separation, reduced the flow distortion by a factor of 10 or more, and improved the pressure recovery. Figure 13 shows isosurface of the total pressure in the channel and pressure recovery contours in the AIP. Table 5 summarizes the results. Comparing the pressure losses of the VG5 and VG9 configurations in Fig. 13 one can see that the VG row 2 in the VG9 configuration generates a secondary flow from the bottom of the channel. It eliminates the vortical structure along the side of the channel and reduces the area of lower total pressure after the first bend. At the same time this secondary flow increases the amount of air in the upper part of the channel in front of the VG row 2. As a result the lower total pressure in the lower part of the AIP, visible for the VG5 configuration, is reduced whereas the pressure losses on the sides of the AIP are larger. The VG9 configuration has somewhat larger values of distortion and, as expected, slightly lower value of pressure recovery but is more stable at different flow conditions.

The model of the inlet with sharp lips and forebody shown in Fig. 10a was tested in the FOI wind tunnel. Because the time and financial sources were rather limited, only subscale Reynolds number tests were carried out. The freestream Mach number was $M = 0.85$. To compensate thicker boundary layer due to subscale Reynolds number, the vortex generator height was increased to keep ratio of $h/\delta \approx 0.3$ based on estimated thickness of the boundary layer.

The analysis of the wind tunnel tests with flow control revealed the presence of two vortices in the lower sector of the AIP not visible in the CFD solution (see Fig. 14). It was lately found out that it is a consequence of the flow separation on the lower side of the channel caused by stronger retardation of the boundary layer on the model forebody. It is evident that moving the vortex generator row VG 2 upstream, the location of this separation would be needed. The flow through the inlet with flow control at all three Reynolds number exhibited large unsteadiness. Final picture of the pressure losses in the AIP is an averaged picture of several snapshots. For Reynolds number $Re = 2.9 \times 10^6$ and $Re = 7.0 \times 10^6$ the pressure distortion was reduced from $DC_{60} = 53\%$ to approximately $DC_{60} \approx 22\text{--}25\%$; for Reynolds number $Re = 5.9 \times 10^6$ the distortion was successfully reduced to $DC_{60} \approx 12\%$ (see Table 6). The improvement of pressure recovery in the inlet with flow control is very small compared to the CFD predictions and occurs only at higher Reynolds numbers. It suggests that the pressure losses in remaining regions of separation are still rather large. Presence of viscous effects on the vortex generators and low values of the Reynolds number reduce the pressure recovery also. Although the tests were carried out at substantially lower Reynolds numbers than those of full scale, the

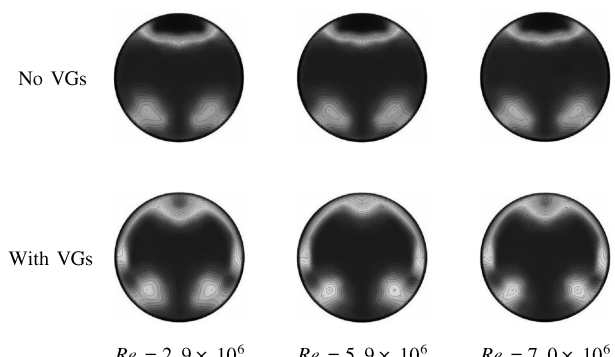


Fig. 14 Total pressure on AIP without and with flow control, wind tunnel data.

evident reduction of distortion suggests that methodology derived during CFD optimization has been useful.

VI. Conclusions

This article deals with an optimization study of the vortex generator flow control in the RAE M2129 inlet and a more complicated inlet used in a UAV. The primary goal is to develop procedures needed for the optimization of vortex generator flow control and to contribute to the understanding of this type of flow control. The study revealed several important findings about VG flow control, namely:

1) The VG flow control geometrical parameters seem to be primarily determined by two flow parameters: the boundary layer thickness in front of separation and the location of the flow separation.

2) The functionality of the VG flow control strongly depends on the vortex generator relative height h/δ and its position towards separation Δx .

3) It is relatively weakly dependent on the vortex generator length l and spacing s .

4) The pressure distortion is independent of the inclination angle of the vortex generator row α_p .

5) The parameters derived for one configuration seem to be transferable to other similar configurations.

From the design methodology point of view, the study shows a substantial effect of different coding of the same parameters. Unlike the set of dimensional parameters, the nondimensional set of parameters led to a construction of relevant response surface. Whether the main cause is a different space filling property of the design or the strong dependence of distortion on the term $1/h$ remains unclear.

Acknowledgments

This work was financed by the Swedish Defence Materiel Administration, FMV. Marlene Johansson of FOI is acknowledged for giving permission to show FOI-EIC-01 study results. The author would like to express thanks to Anthony A. Giunta of Sandia National Laboratories, New Mexico, for his useful comments and suggestions on this report. Thanks to Stefan Jakobsson of FOI for help with Matlab scripts used during construction of the response surfaces. Stephen Conway of Scania and Mattias Chevalier of FOI are acknowledged for many comments and the excellent work during revision of this article.

References

- [1] Miller, D., and Addington, G., "Invited: Aerodynamic Flowfield Control Technologies for Highly Integrated Airframe Propulsion Flowpaths," AIAA Paper 2004-2625, June 2004.
- [2] Hamstra, J. W., Miller, D. N., Traux, P. P., Anderson, B. H., and Wend, B. J., "Active Inlet Flow Control Technology Demonstration," ICAS Paper 2000-6.11.2, Aug.–Sept. 2000.
- [3] Mattingly, J., Heiser, W., and Pratt, D., *Aircraft Engine Design*, 2nd ed., AIAA Education Series, American Institute of Aeronautics and Astronautics, Reston, VA, 2002.
- [4] Daggett, D. L., Kawai, R., and Friedman, D., "Blended Wing Body Systems Studies: Boundary Layer Ingestion Inlets with Active Flow Control," NASA CR-2003-212670, Dec. 2003.
- [5] Campbell, R. L., Carter, M. B., Pendegraft, O. C., Friedman, D. M., and Serrano, L., "Design and Testing of a Blended Wing Body with Boundary Layer Ingestion Nacelles at High Reynolds Numbers (Invited)," AIAA Paper 2005-459, June 2005.
- [6] Aerospace Information Report, "Inlet Total-Pressure-Distortion Considerations for Gas-Turbine Engines," Aerospace Council Division, Society of Automotive Engineers, Inc., AIR 1419, 1983.
- [7] Kaldschmidt, G., Syltebo, B. E., and Ting, C. T., "A 727 Airplane Center Duct Inlet Low Speed Performance Confirmation Model Test for Refanned JT8D Engines, Phase 2," NASA CR-134534, Nov. 1973.
- [8] Anderson, B. H., Huang, P. S., Paschal, W. A., and Cavatorta, E., "Study of Vortex Flow Control of Inlet Distortion," *Journal of Propulsion and Power*, Vol. 8, No. 6, 1992, pp. 1266–1272.
- [9] Anderson, B. H., and Gibb, J., "Vortex Generator Installation of Steady State and Dynamic Distortion," AIAA Paper 1996-3279, June 1996.
- [10] Anbtawi, A. J., Blackwelder, R. F., Lissaman, P. B. S., and Liebeck, R. H., "An Experimental Investigation of Boundary Layer Ingestion in a Diffusing S-Duct with and Without Passive Flow Control," AIAA Paper 1999-0739, Jan. 1999.
- [11] Allan, B. G., and Owens, L. R., "Numerical Modelling of Flow Control in a Boundary-Layer-Ingesting Offset Inlet Diffusers at Transonic Mach Numbers," AIAA Paper 2006-0845, Jan. 2006.
- [12] Allan, B. G., Owens, L. R., and Lin, J. C., "Optimal Design of Passive Flow Control for a Boundary-Layer-Ingesting Offset Inlet Using Design-of-Experiments," AIAA Paper 2006-1049, Jan. 2006.
- [13] Owens, L. R., Allan, B. G., and Gorton, S. A., "Boundary-Layer-Ingesting Inlet Flow Control," AIAA Paper 2006-839, Jan. 2006.
- [14] Dudek, J. C., "Empirical Model for Vane-Type Vortex Generators in a Navier–Stokes Code," *AIAA Journal*, Vol. 44, No. 8, Aug. 2006, pp. 1779–1789.
- [15] Myers, R. H., and Montgomery, D. C., *Response Surface Methodology —Process and Product Optimization Using Designed Experiments, Probability and Statistics*, 3rd ed., John Wiley and Sons, New York, 1995.
- [16] Schmidt, R., and Laundsby, T., *Understanding Design of Experiment*, Academy Associates, Colorado Springs, CO, 1995.
- [17] Giunta, A. A., Wojtkiewicz, S. F., and Eldred, M. S., "Overview of Modern Design of Experiments Methods for Computational Simulations," AIAA Paper 2003-649, Jan. 2003.
- [18] Anderson, B. H., and Keller, D. J., "A Robust Design Methodology for Optimal Microscale Secondary Flow Control in Compact Inlet Diffusers," NASA TM 2002-211477, June 2002.
- [19] Anderson, B. H., and Keller, D. J., "Consideration in the Measurement of Inlet Distortion for High Cycle Fatigue in Compact Inlet Diffusers," NASA TM 2002-211476, June 2002.
- [20] Anderson, B. H., and Keller, D. J., "A Parameter Design Methodologies for Micro-Scale Secondary Flow Control in Compact Inlets," AIAA Paper 2002-0541, June 2002.
- [21] Anderson, B. H., Yagle, P. J., Miller, D. N., and Traux, P. P., "A Study of MEMS Flow Control for the Management of Engine Distortion in Compact Inlet Systems," FEDSM Paper 99-6920, July 1999.
- [22] Anderson, B. H., Miller, D. N., and Abd J. Agrell, M. C. G., "The Role of Design-of-Experiments in Managing Flow in Compact Air Vehicle Inlets," NASA TM 2003-212601, Sept. 2003.
- [23] Jirásek, A., "Vortex-Generator Model and its Application to Flow Control," *Journal of Aircraft*, Vol. 42, No. 6, Nov.–Dec. 2005, pp. 1486–1491.
- [24] Montgomery, D. C., *Response Surface Method*, 5th ed., John Wiley and Sons, New York, 1995.
- [25] Giunta, A. A., "Aircraft Multidisciplinary Design Optimization Using Design of Experiments Theory and Response Surface Modeling Methods," Ph.D. Thesis, Virginia Polytechnic Institute, Blacksburg, VA, May 1997.
- [26] Simpson, T. W., Korte, J. J., Maurey, T. M., and Mistree, F., "Comparison of Response Surface and Kriging Models for Multidisciplinary Design Optimization," AIAA Paper 1998-4755, Jan. 1998.
- [27] Eliasson, P., "EDGE, a Navier–Stokes Solver for Unstructured Grids," *Proceedings to Finite Volumes for Complex Applications III*, edited by D. Kröner and R. Herbin, Hermès Penton Science, London, 2002, pp. 527–534.
- [28] Wallin, S., and Johansson, A. V., "A Complete Explicit Algebraic Reynolds Stress Model for Incompressible and Compressible Turbulent Flows," *Journal of Fluid Mechanics*, Vol. 403, 2000, pp. 89–132.
- [29] Jirásek, A., "Mass Flow Boundary Conditions for Subsonic Inflow and Outflow Boundary," *AIAA Journal*, Vol. 44, No. 5, May 2006, pp. 939–947.
- [30] Advisory Group for Aerospace Research & Development, "Air Intakes for High Speed Vehicles," Fluid Dynamics Panel Working Group 13, AGARD AR-270, 1991.
- [31] Seddon, J. J., and Goldsmith, E. L., *Intake Aerodynamics*, 3rd ed., AIAA, Washington, DC, 1995.
- [32] Daniel, C., "Use of Half-Normal Plots in Interpreting Factorial Two Level Experiment," *Technometrics*, Vol. 1, No. 4, 1959, pp. 311–341.
- [33] Box, G. E. P., and Meyer, R. D., "An Analysis of Unreplicated Fractional Factorials," *Technometrics*, Vol. 28, No. 1, 1986, pp. 11–18.
- [34] Montgomery, D. C., Peck, E. A., and Vining, G. G., *Introduction to Linear Regression Analysis*, 3rd ed., John Wiley and Sons, New York, 2001.
- [35] Johansson, M., "FoT25 2003–2005 Propulsion Integration, Final Report," FOI R-1572-SE, Dec. 2005.